Am J Physiol Gastrointest Liver Physiol
281: G1477–G1486, 2001.

Intracellular trafficking/membrane targeting of human reduced folate carrier expressed in *Xenopus* oocytes

VEEDAMALI S. SUBRAMANIAN*,[1–3] JONATHAN S. MARCHANT*,[4]
IAN PARKER,[4] AND HAMID M. SAID[1–3]
[1]*Department of Veterans Affairs Medical Center, Long Beach 90822;*
and Departments of [2]*Medicine,* [3]*Physiology/Biophysics, and* [4]*Neurobiology*
and Behavior, University of California, Irvine, California 92697

Received 9 August 2001; accepted in final form 4 September 2001

Subramanian, Veedamali S., Jonathan S. Marchant, Ian Parker, and Hamid M. Said. Intracellular trafficking/membrane targeting of human reduced folate carrier expressed in *Xenopus* oocytes. *Am J Physiol Gastrointest Liver Physiol* 281: G1477–G1486, 2001.—The major cellular pathway for uptake of the vitamin folic acid, including its absorption in the intestine, is via a plasma membrane carrier system, the reduced folate carrier (RFC). Very little is known about the mechanisms that control intracellular trafficking and plasma membrane targeting of RFC. To begin addressing these issues, we used *Xenopus* oocyte as a model system and examined whether the signal that targets the protein to the plasma membrane is located in the COOH-terminal cytoplasmic tail or in the backbone of the polypeptide. We also examined the role of microtubules and microfilaments in intracellular trafficking of the protein. Confocal imaging of human RFC (hRFC) fused to the enhanced green fluorescent protein (hRFC-EGFP) showed that the protein was expressed at the plasma membrane, with expression confined almost entirely to the animal pole of the oocyte. Localization of hRFC at the plasma membrane was not affected by partial or total truncation of the COOH-terminal tail of the polypeptide, whereas a construct of the cytoplasmic tail fused to EGFP was not found at the plasma membrane. Disruption of microtubules, but not microfilaments, prevented hRFC expression at the plasma membrane. These results demonstrate that the molecular determinant(s) that directs plasma membrane targeting of hRFC is located within the backbone of the polypeptide and that intact microtubules, but not microfilaments, are essential for intracellular trafficking of the protein.

folate membrane transporter; cell biology

THE COENZYME DERIVATIVES of folic acid are necessary for the synthesis of purine and pyrimidine precursors of nucleic acids, the metabolism of certain amino acids, and initiation of protein synthesis in mitochondria (3, 40). Mammals cannot synthesize folate and must obtain the vitamin from exogenous sources via intestinal absorption followed by distribution to different cell types. The major pathway for cellular uptake of folate (including its absorption in the small intestine) occurs via a specialized plasma membrane carrier system (24, 35–37) identified as the reduced folate carrier (RFC) (8, 27, 29, 44, 45). To date, RFCs have been cloned from several species including human (27, 29, 45), mouse (8), hamster (44), and rat (S. A. Rubin, Dept. of Medicine, Univ. of California at Los Angeles, Los Angeles, CA; GenBank accession no. U38180) and have been shown to be integral membrane proteins with 12 predicted transmembrane domains (12, 37). The human RFC (hRFC) protein has 591 amino acids with a long (139 amino acids) cytoplasmic COOH-terminal tail (12, 37). Functional identity of the cloned RFCs has been confirmed by expression in mammalian cells (12, 20, 37, 43) and *Xenopus* oocytes (20).

In contrast to our knowledge of the molecular identity, functional properties, and distribution of the RFC uptake system, little is known about the mechanisms that control intracellular trafficking and membrane targeting of RFC. Recent studies investigating the membrane targeting of a variety of transporters demonstrated the involvement of specific molecular determinants (motifs/residues, e.g., tyrosine/leucine) responsible for guiding their delivery to the plasma membrane (4, 5, 25). In many cases, these motifs/residues are located within the COOH-terminal cytoplasmic tail of the polypeptide (see, e.g., Refs. 19, 23, 28); in other cases, however, the location was found in the backbone sequence of the polypeptide (2, 17, 18). In the case of hRFC, this polypeptide appears to have a number of such candidate targeting signals (e.g., leucine/tyrosine motifs) both within its backbone sequence and within the COOH-terminal cytoplasmic tail. Furthermore, other studies have shown that the cytoskeletal network plays an important role in the intracellular trafficking of membrane transporters to the cell surface (1, 4, 9, 13). Therefore, we were interested in identifying the domains and molecular signals that target hRFC to the plasma membrane and in assessing the role of the cytoskeleton in the intracellular trafficking of hRFC in different cells.

*V. S. Subramanian and J. S. Marchant contributed equally to this work.

Address for reprint requests and other correspondence: H. M. Said, VA Medical Center, Long Beach, CA 90822 (E-mail: hmsaid@uci.edu).

The costs of publication of this article were defrayed in part by the payment of page charges. The article must therefore be hereby marked "*advertisement*" in accordance with 18 U.S.C. Section 1734 solely to indicate this fact.

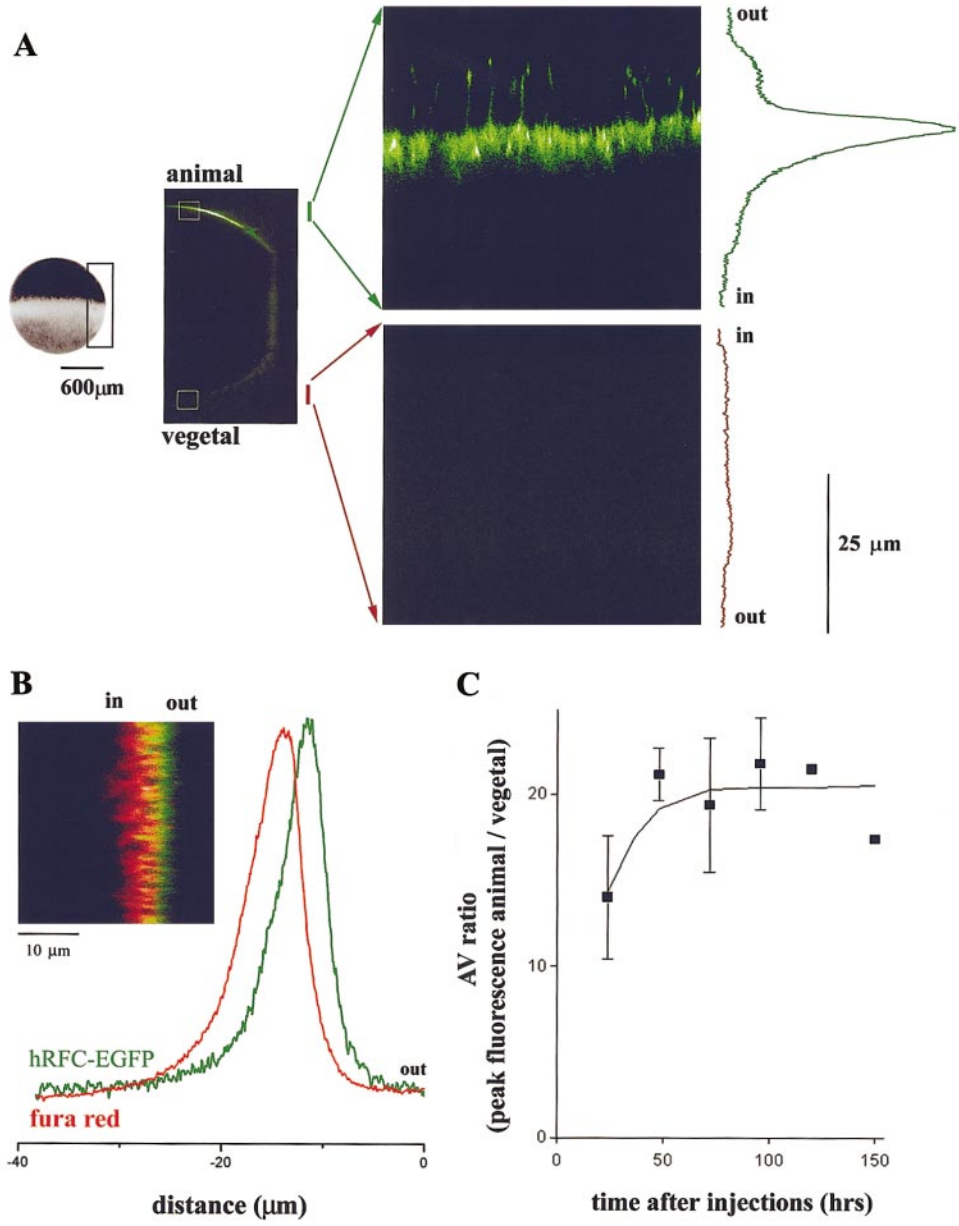

Fig. 1. Expression of human reduced folate carrier (hRFC)-enhanced green fluorescent protein (EGFP) cDNA in *Xenopus* oocytes. *A*: *Far left*, a bright-field image of a pigmented *Xenopus* oocyte indicating the orientation of the oocyte in the confocal fluorescence images. *Center left*, a low-power (×10, dry objective) axial (*x*-*z*) confocal fluorescence image of an oocyte microinjected 48 h previously with hRFC-EGFP cDNA and orientated as depicted on a cover glass (flattened part of oocyte). *Right*, higher-resolution (×40 oil-immersion objective) axial scans into the animal (*top*, white box) and vegetal pole (*bottom*, white box) hemispheres. Traces (*far right*) represent fluorescence intensity as a function of depth into the oocyte averaged across a 40-μm section of the laser scan line. *B*: dual-emission axial scan (*x*-*z*) of an hRFC-EGFP-expressing oocyte previously microinjected with fura red (30 μM final concentration). hRFC-EGFP fluorescence was monitored using a 530 ± 20-nm bandpass filter, and fura red fluorescence was monitored at λ > 620 nm. Traces show average fluorescence intensity across the scan line with increasing depth into the oocyte. *C*: quantification of animal-to-vegetal polarity (A/V ratio) was estimated at different times after microinjection from the ratio of peak fluorescence intensity from $n > 3$ scans in the animal and vegetal hemispheres of the same oocyte. Measurements are from oocytes that displayed fluorescence 24 h after nuclear injection of hRFC-EGFP cDNA. Data are means ± SE from 40 oocytes, 10 donor animals.

To begin addressing these issues, we sought in the present study to determine the location of the membrane-targeting signal of hRFC to sequence within the long COOH-terminal cytoplasmic tail of the protein or, alternatively, to sequence in the preceding backbone region of the polypeptide. We also determined the role of microtubules and microfilaments in the intracellular trafficking of hRFC. We used the *Xenopus* oocyte as an in vitro model system, because it faithfully expresses RFC (29) and other exogenous proteins and because of its convenient size and established utility in similar studies with other transporters (10, 14). Our results show that hRFC fused to the enhanced green fluorescent protein (hRFC-EGFP) is functionally expressed at the plasma membrane of *Xenopus* oocytes, with the majority of expression localized to the animal hemisphere. Deletion of the COOH-terminal cytoplasmic tail did not affect targeting of hRFC to the plasma membrane, whereas a construct of COOH-terminal cytoplasmic tail fused to EGFP was not found at the plasma membrane. These findings suggest that the membrane-targeting signal of hRFC is located in the backbone of the polypeptide. Furthermore, our results show that the intracellular trafficking of hRFC is critically dependent on intact microtubules but not microfilaments.

MATERIALS AND METHODS

Materials. [3′,5′,7,9-^{3}H(N)]folinic acid (specific activity, 12.7 Ci/mmol) was obtained from Moravek Biochemicals (Brea, CA). Fura red was from Molecular Probes (Eugene, OR). The fluorescent protein constructs [enhanced yellow fluorescent protein (EYFP)-endoplasmic reticulum (ER), EYFP-actin, EGFP-tubulin, and EGFP-aminoterminus (N3)]

were from Clontech (Palo Alto, CA). Cytochalasin D and nocodazole were from Calbiochem (La Jolla, CA). All other reagents were obtained from suppliers as outlined previously (29, 31).

Construction of hRFC-EGFP and truncated constructs. The coding region of the full-length hRFC and its truncated constructs were generated by PCR using combinations of the following primers: F1 (5′CCGCTCGAGATGGTGCCCTCCAGCCCAGCG3′), F2 (5′CCGCTCGAGATGGCCTGCGGCACT-GCC3′), R1 (5′CGGGATCCCTGGTTCACATTCTGAACACCG3′), R2 (5′CGGGATCCGGCC-GGGGCCTGGGCCAG3′), and R3 (5′CGGGATCCCAGC-ATGGCCCCCAAGAAGTAG3′). For the full-length hRFC [base pairs (bp) 1–1773, corresponding to amino acids 1–591], primers F1 and R1 were used. For the hRFC construct with a partially truncated COOH-terminal cytoplasmic tail (bp 1–1590, corresponding to amino acids 1–530), primers F1 and R2 were used. For the hRFC construct with total truncation of the COOH-terminal cytoplasmic tail (bp 1–1356, corresponding to amino acids 1–452), primers F1 and R3 were used. We also prepared a construct of the COOH-terminal cytoplasmic tail of the hRFC alone (bp 1357–1773, corresponding to amino acids 452–591) using primers F2 and R1. In all cases, EGFP was fused to the COOH terminus of hRFC. Briefly, the PCR conditions were 94°C for 3 min, followed by 33 cycles of 30 s at 94°C, 30 s at 55°C, and 4 min at 68°C, with a final 10 min at 68°C to yield products of 1,773, 1,590, 1,356, and 417 bp. The PCR products and the EGFP-N3 vector were then digested with *Bam*HI and *Xho*I, and the products were gel isolated and ligated together, generating in-frame fusion proteins under the control of the human cytomegalovirus promoter. The nucleotide sequence of each construct was confirmed by sequencing (SeqWright, Houston, TX). The amino acid sequence of the resulting constructs is shown schematically in Fig. 4*A*.

Procurement and nuclear microinjection of Xenopus oocytes. Female adult *Xenopus laevis* frogs were anesthetized by immersion in 0.1% aqueous solution of 3-aminobenzoic acid ethyl ester (MS-222) for 15 min, and after death by decapitation, whole ovaries were removed. The epithelial layers of stage VI oocytes (11) were removed using watchmakers' forceps, and oocytes were then treated with collagenase (0.5 mg/ml for 30 min) in dissociation solution (in mM: 82.5 NaCl, 2.5 KCl, 10 Na_2HPO_4, and 5 HEPES, pH 7.8) to

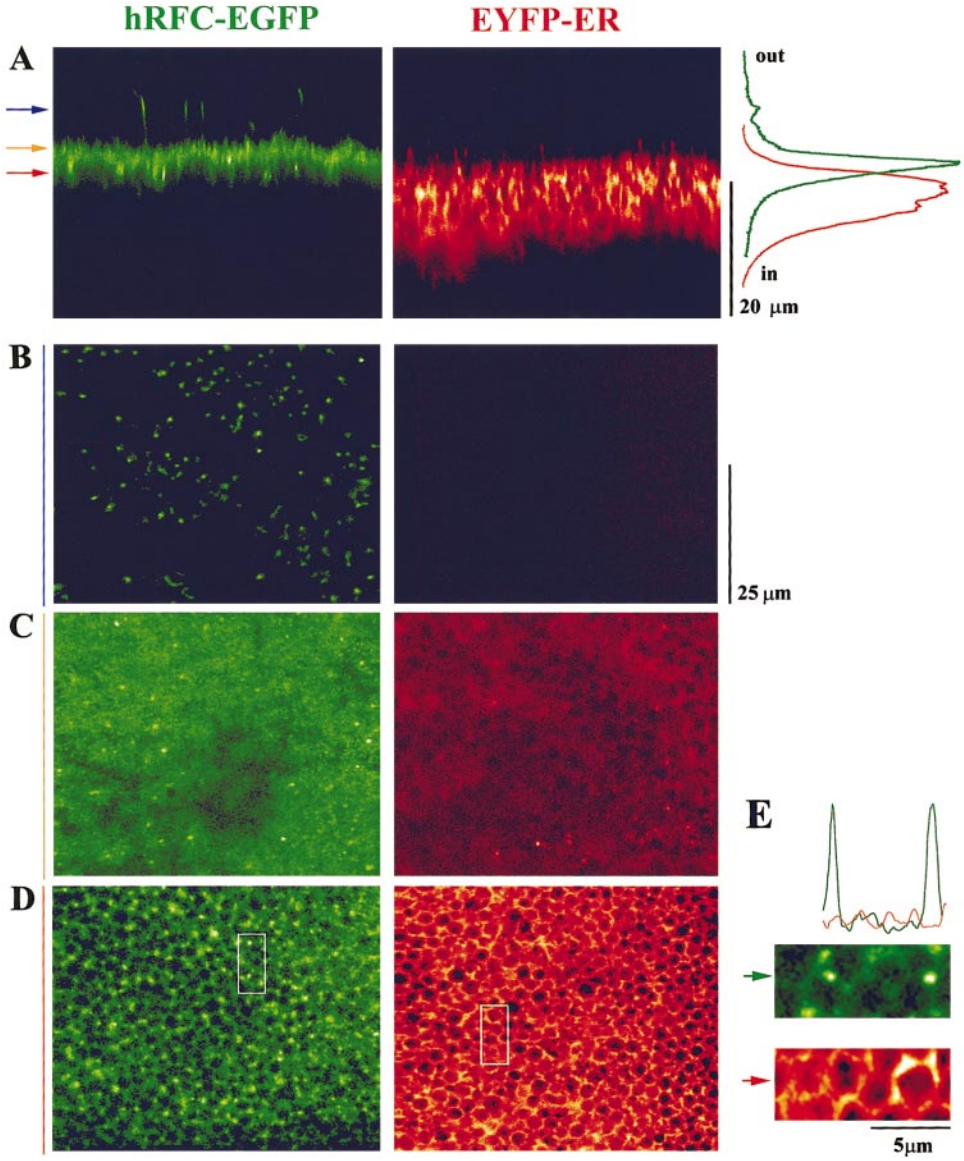

Fig. 2. hRFC-EGFP localization within the *Xenopus* oocyte plasma membrane and endoplasmic reticulum (ER). *A*: Axial (*x*-*z*) scans of oocytes expressing hRFC-EGFP and enhanced yellow fluorescent protein (EYFP)-ER. Traces (*right*) depict the fluorescence intensity averaged along a 40-μm section of the 50-μm laser scan line in oocytes expressing hRFC-EGFP (green) or EYFP-ER (red). Arrows (*left*) show the position of lateral (*x*-*y*) confocal scan presented in *B*, *C*, and *D*, which are representative of peripheral microvilli, plasma membrane, and cortical ER, respectively, in oocytes expressing hRFC-EGFP and EYFP-ER. *E*: enlarged views from *D* illustrating morphology at the level of the ER in oocytes expressing hRFC-EGFP (green) and EYFP-ER (red). Traces from separate cells represent the intensity profile across a 3-pixel-wide line, as indicated by the arrow and scaled on the same color table, indicating the punctate vesicularized fluorescence of hRFC-EGFP (green) relative to the more homogeneous fluorescence of EYFP-ER (red).

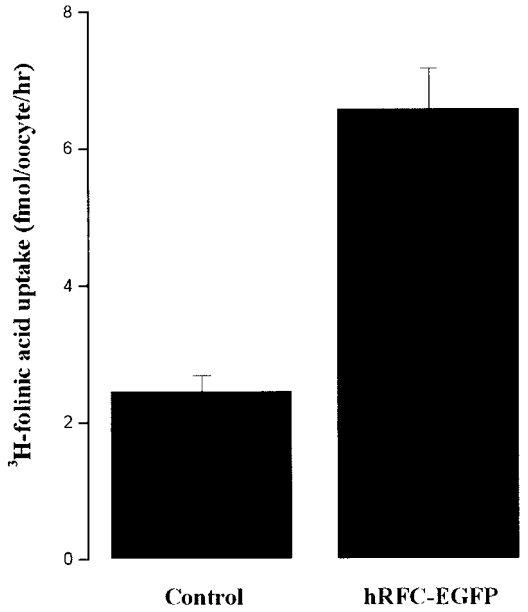

Fig. 3. hRFC is functionally expressed within the oocyte plasma membrane. Uptake of [^{3}H]folinic acid in mock-injected (control) and hRFC-EGFP-injected oocytes assayed 48–72 h after nuclear injection of cDNA. Results represent means ± SE from 3 donor animals.

ensure complete defolliculation. Oocytes were left to recover for 24 h before microinjection. For expression studies, ~2 ng of plasmid cDNA in 5 nl of intracellular solution (in mM: 140 KCl, 10 HEPES, 3 $MgCl_2$, 1 EGTA, and 0.5 $CaCl_2$, pH 7.3) were injected with a Drummond microinjector into the nucleus of each oocyte. Injected oocytes were separated and maintained in Barth's solution [88 mM NaCl, 1 mM KCl, 2.4 mM $NaHCO_3$, 0.83 mM $MgSO_4$, 0.33 mM $Ca(NO_3)_2$, 0.41 mM $CaCl_2$, 10 mM HEPES, 550 mg/l Na pyruvate, and 0.05 mg/ml gentamycin; pH 7.4 at 18°C] with repeated changes of solution at least every 12 h. Additional oocytes from the same donor were injected with ~5 nl of intracellular solution and maintained as parallel controls for viability and uptake assays.

Assay of [^{3}H]folinic acid uptake. With methods reported previously (29), batches of eight oocytes that scored positive for EGFP fluorescence (48–72 h after microinjection) were incubated at room temperature for 1 h in 200 μl of Barth's solution supplemented with 120 nM [^{3}H]folinic acid. Uptake was terminated by addition of 5 ml of ice-cold Barth's solution. Oocytes were transferred individually to scintillation vials and dissolved in 250 μl of 10% SDS before addition of scintillation fluid.

Confocal imaging of hRFC constructs. Oocytes were monitored for hRFC-EGFP expression using a custom-built laser scanning confocal microscope based on an Olympus IX70 inverted microscope fitted with a 40× oil-immersion objective (31). EGFP was excited using the 488-nm line from an argon ion laser, and emitted fluorescence was monitored with a 530 ± 20-nm bandpass filter. Autofluorescence (monitored in mock-injected oocytes) was negligible (<2%) compared with oocytes expressing EGFP-tagged constructs. Confocal images were obtained by scanning the laser scan line either laterally (*x-y* scans) or axially (*x-z* scans) within the oocyte. All measurements of EGFP fluorescence were averaged from more than six independent scans in several oocytes from more than three donor frogs, and all results are presented as means ± SE. All fluorescence images were collected at room temperature with the oocytes bathed in Barth's solution.

RESULTS

Expression of hRFC-EGFP in Xenopus oocytes. To investigate the targeting of hRFC by the endogenous protein trafficking mechanisms within *Xenopus* oocytes, we injected cDNA encoding hRFC-EGFP into the nucleus of stage VI oocytes. Two days after microinjection, oocytes were imaged by confocal microscopy for expression of hRFC-EGFP. In all oocytes examined (n = 40 oocytes, 10 donor animals) hRFC-EGFP fluorescence was confined to the animal hemisphere (Fig. 1*A*), with an average 15.5 ± 2.5-fold greater peak fluorescence in the animal compared with the vegetal pole (n = 40 cells, 10 donors). Little, if any, EGFP fluorescence was detectable in the vegetal hemisphere, as fluorescent intensities were similar to autofluorescence in the vegetal hemisphere of mock-injected oocytes maintained as parallel controls (data not shown). Within the animal hemisphere, hRFC-EGFP expression was confined to a radial band 5.6 ± 1.2 μm wide [full width at half-maximal intensity; n = 40 cells, 10 donors], consistent with the dimensions of the highly convoluted oocyte plasma membrane. Furthermore, hRFC-EGFP fluorescence was localized more superficially than red fluorescence observed with a microinjected cytosolic marker (fura red, 30 μM), suggesting that the majority of expressed hRFC-EGFP was targeted to the plasma membrane (Fig. 1*B*).

The fluorescence ratio between the animal and vegetal hemispheres was monitored at various times (<150 h) after nuclear injection. The pronounced asymmetry in hRFC-EGFP expression was evident as soon

Fig. 4. Targeting of truncated hRFC-EGFP mutants. *A*: schematic representation of the amino acid sequence of hRFC-EGFP and 3 truncated fusion constructs. The NH_2-terminal (dotted line), transmembrane domain (TD), and COOH-terminal domain (solid line) of hRFC are illustrated relative to the amino acid sequence of full-length hRFC. hRFC, F1-R2, F1-R3, and F2-R1 represent the full-length sequence of hRFC, hRFC with a partial truncation of the cytoplasmic COOH-terminal tail, hRFC with a total truncation of the cytoplasmic COOH-terminal tail, and the cytoplasmic COOH-terminal tail of hRFC alone, respectively, all fused with EGFP. *B*: targeting of truncated hRFC-EGFP mutants. Representative axial (*x-z*) scans (50-μm laser line) from the animal and vegetal poles of oocytes microinjected with F1R2 (*i*, *ii*), F1R3 (*iii*, *iv*) and F2R1 (*v*, *vi*). Traces (*right*) show the corresponding fluorescence profile averaged across a 40-μm-wide section of the laser scan line with depth in the animal (green) and vegetal (brown) hemispheres of oocytes expressing the indicated construct. *C*: measurements of the A/V fluorescence ratio from images such as those presented in *B*. Measurements for the F1R2 construct are not applicable (shown as "n/a" on figure), because no fluorescence was detectable in oocytes injected with this construct. *D*: measurement of the full width at half-maximal fluorescence intensity of the fluorescence profile (FWHM) in the animal hemisphere of oocytes expressing different truncated constructs (filled bars) relative to hRFC-EGFP (open bar). Measurements are from a total of n >10 oocytes, n > 3 donors for each construct.

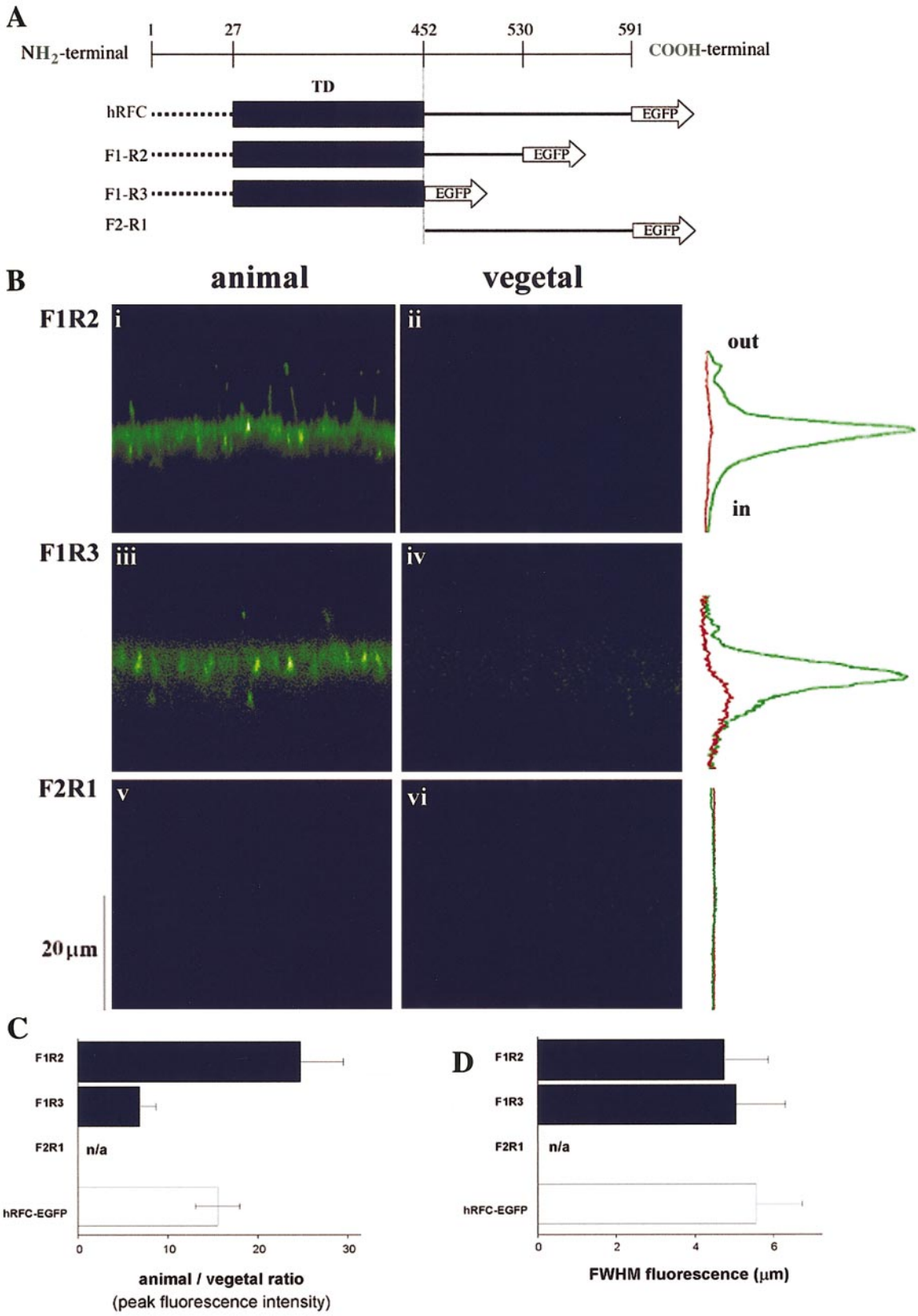
A
1
27
452
530
591
NH2-terminal
COOH-terminal
TD
hRFC
F1-R2
F1-R3
F2-R1
EGFP
B
animal
vegetal
F1R2
i
ii
out
in
F1R3
iii
iv
F2R1
v
vi
20 μm
C
F1R2
F1R3
F2R1
n/a
hRFC-EGFP
0
10
20
30
animal / vegetal ratio
(peak fluorescence intensity)
D
F1R2
F1R3
F2R1
n/a
hRFC-EGFP
0
2
4
6
FWHM fluorescence (μm)

as fluorescence was detectable (~24 h) and increased to a stable ratio of ~15–20, which was maintained over at least a 7-day period (Fig. 1*C*).

Distribution of hRFC-EGFP within animal hemisphere. To image the subcellular distribution of hRFC-EGFP within the animal hemisphere of the oocyte, we collected lateral (*x-y*) confocal images at increasing depths into the oocyte (Fig. 2*A*) and compared this distribution to that observed with an ER-targeted EYFP construct (EYFP-ER). The fluorescence distribution with each of these constructs was clearly different (Fig. 2), with the presence of microvilli and the peripheral localization of hRFC-EGFP within confocal sections (Figs. 1 and 2) strongly suggesting plasma membrane localization. Most obviously, in oocytes in which surface structure was well preserved after collagenase treatment, hRFC-EGFP expression was evident in long microvilli (up to ~10-μm length) projecting superficially from the plasma membrane (Fig. 2*A*), which appeared as ~0.5-μm-wide cylinders in cross section (Fig. 2*B*). The fluorescence signal of hRFC-EGFP became more uniform within the plasma membrane proper, at which depth ER structure first became visible (Fig. 2*C*). Further inside the oocyte, hRFC-EGFP was resolved as highly punctate vesicular structures (~0.6 μm in diameter) located within a more diffusively stained network (Fig. 2, *D* and *E*). These vesicles were also evident in axial (*x-z*) sections in which individual vesicles were transected by the laser scan line (see, e.g., Fig. 2*A*). This network was most likely the cortical ER of the oocyte, because the fluorescence signal in oocytes expressing EYFP-ER displayed an anastomosing network of tubules at this same level (Fig. 2, *D* and *E*). Therefore, it is likely that the bright punctate structures represent hRFC-EGFP localized within trafficking vesicles that are being transported through the ER to the cell surface.

hRFC-EGFP is functionally expressed in plasma membrane. Implicit in these studies is the verification that fusion of hRFC with EGFP (27 kDa) does not alter the normal plasma membrane targeting and activity of hRFC (12, 41). This was confirmed by measurements of [^{3}H]folinic acid uptake, showing levels 2.7-fold higher in oocytes expressing hRFC-EGFP cDNA compared with the endogenous uptake in water-injected controls (Fig. 3; 6.58 ± 0.59 vs. 2.45 ± 0.24 fmol·oocyte^{-1}·h^{-1}, respectively). These data are consistent with a 2.4-fold enhancement of uptake reported previously in oocytes injected with cRNA encoding hRFC alone (29). Together, the results from Figs. 1, 2, and 3 confirm that EGFP tagging of hRFC affects neither its localization at the plasma membrane nor the functional ability of hRFC to transport folinic acid.

Relative importance of COOH-terminal cytoplasmic tail of hRFC compared with backbone sequence in targeting protein to plasma membrane. In this study, we examined whether the motif(s)/signal(s) that determines membrane targeting of the hRFC protein is endowed to a sequence at the COOH-terminal cytoplasmic tail of the protein or to a sequence in the backbone region of the polypeptide. To do so, we designed two hRFC constructs fused to EGFP with partial (F1R2: amino acids 1–530) or complete (F1R3: amino acids 1–452) truncation of the COOH-terminal cytoplasmic tail (Fig. 4*A*). We also designed an EGFP-fusion protein of the COOH-terminal sequence alone (F2R1: amino acids 452–591).

Figure 4*B* shows representative confocal axial (*x-z*) images taken in the animal and vegetal hemispheres of oocytes microinjected with F1R2, F1R3, and F2R1. Whereas F1R2 and F1R3 were like full-length hRFC-EGFP asymmetrically expressed across the oocyte cell membrane, quantitative differences in the ratio of expression across the oocyte (peak fluorescence intensity in animal hemisphere vs. vegetal hemisphere) were observed (Fig. 4*C*). With F1R2, the peak fluorescence intensity in the animal hemisphere was 28.3 ± 5.4-fold greater than in the vegetal hemisphere (n = 28 cells, 5 donors), whereas the asymmetry was less pronounced (7.9 ± 2.0-fold) in oocytes expressing F1R3 (n = 16 cells, 5 donors). However, both constructs were targeted to the plasma membrane, displaying a width of fluorescence signal (Fig. 4*D*) and a morphological appearance similar to those observed with hRFC-EGFP. With regard to the F2R1 construct (Fig. 4*B*), no fluorescence was detected at the plasma membrane of oocytes.

Role of cytoskeleton in hRFC localization. If the cytoskeleton plays a role in intracellular trafficking of hRFC-EGFP to the plasma membrane, then a simple explanation for the observed asymmetric distribution of hRFC-EGFP could be a polarized distribution of cytoskeletal filaments across the oocyte. We therefore performed separate nuclear injections of plasmids en-

Fig. 5. Morphology of the cortical cytoskeleton and effects of cytoskeletal disruption on hRFC-EGFP trafficking in *Xenopus* oocytes. *A*: axial fluorescence images (*x-z*) taken 48 h after microinjection of cDNA constructs to express hRFC-EGFP (*i*, *ii*), EYFP-actin (*iii*, *iv*), and EGFP-tubulin (*v*, *vi*) in the animal and vegetal hemispheres of *Xenopus* oocytes. Traces (*right*) show the fluorescence profile with depth in the animal (green) and vegetal hemispheres (brown) averaged across a 40-μm-wide section of the laser scan line. *B*: the effect of application of nocodazole (10 μM) or cytochalasin D (10 μM) on the expression of hRFC-EGFP. Oocytes were injected with cDNA encoding hRFC-EGFP, and individual batches of 30 cells were treated with either drug or DMSO alone (0.1% solution) beginning at various times after microinjection (3–6, 6–9, and 9–12 h). Oocytes were maintained in this same solution until imaging 30 h after microinjection. Measurements represent % of oocytes within each batch in which EGFP fluorescence was detectable. *C*: *top*, photographs showing the effect of prolonged exposure (>10 h) of oocytes to cytochalasin D (10 μM) and nocodazole (10 μM). *Bottom*, effect of cytoskeletal drugs on the fluorescence intensity at the oocyte surface. Oocytes were exposed to either 10 μM cytochalasin D or 10 μM nocodazole beginning after ~15–20 h, when fluorescence was first detectable at the cell surface. Measurements of hRFC-EGFP fluorescence were taken subsequently as indicated. Data represent the mean fluorescence from several oocytes (n > 3) at each time from n > 3 donor animals.

coding either an EYFP-β-actin fusion construct (EYFP-actin) or an EGFP-α-tubulin fusion construct (EGFP-tubulin). Fig. 5*A* shows axial (*x-z*) scans of the animal and vegetal hemispheres of oocytes from the same donor animal expressing hRFC-EGFP, EYFP-actin, or EGFP-tubulin. In contrast to the striking hemispheric polarity observed with hRFC-EGFP (~15-fold; Figs. 1 and 5), the distribution of both EYFP-actin and EGFP-tubulin was more uniform across the cell. The peak fluorescence of EYFP-actin was only ~1.5-fold greater in the animal compared with the vegetal hemisphere (1.47 ± 0.05-fold, $n = 6$ cells), and the width of the fluorescence signal was similar in animal (6.70 ± 0.51 μm) and vegetal (6.35 ± 0.47 μm) hemispheres. The distribution of EGFP-tubulin paralleled that of EYFP-actin: the peak fluorescence was similarly only ~1.5-

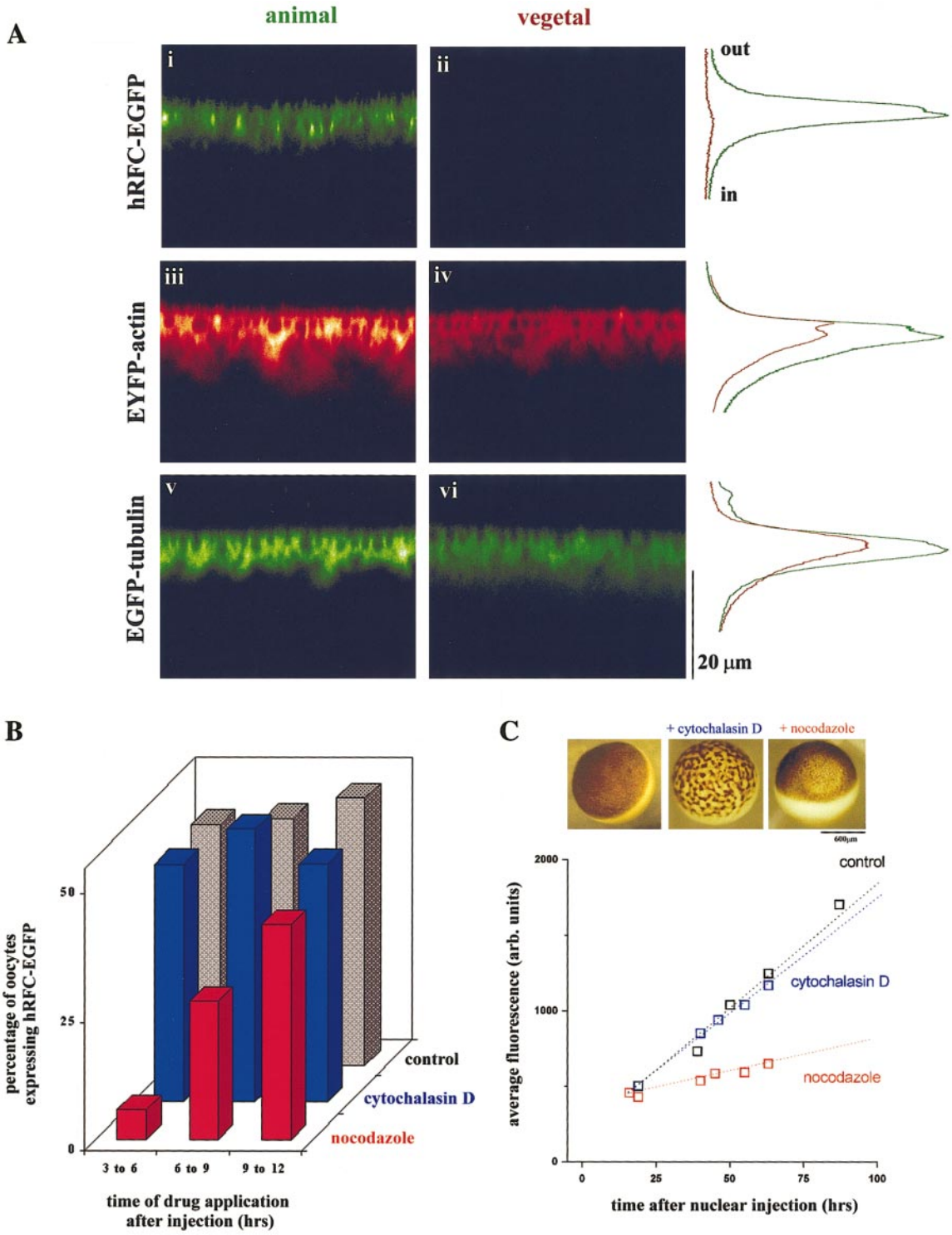

fold greater in the animal hemisphere (1.42 ± 0.15-fold; $n = 8$ oocytes), although the depth of resolution of EGFP-tubulin was greater in the vegetal (8.45 ± 0.23 μm) than the animal (4.91 ± 0.18 μm) hemisphere. In summary, these data demonstrate that the observed distribution of hRFC-EGFP in the oocyte plasma membrane is much more asymmetric than that seen with actin and tubulin.

To investigate the role played by the cytoskeleton in hRFC-EGFP trafficking, we analyzed the effects of disruption of the cytoskeletal architecture of the oocyte by employing the microtubule-disrupting agent nocodazole (15) and the microfilament-disrupting agent cytochalasin D (6, 32). Oocytes were transferred to solutions containing either cytochalasin D (10 μM) or nocodazole (10 μM) at various time points (3–12 h) after nuclear injection of hRFC-EGFP and were subsequently screened for expression after 30 h (i.e., incubation periods of 27–18 h). Incubation of oocytes in cytochalasin D had no effect on the proportion of oocytes expressing hRFC-EGFP, irrespective of the duration of the incubation (Fig. 5*B*). In contrast, nocodazole markedly inhibited the expression of hRFC-EGFP at the cell surface (Fig. 5*B*). Application of nocodazole 3–6 h after nuclear injection resulted in a marked decrease in the number of expressing oocytes relative to the controls (5.8 ± 3.2% vs. 46.9 ± 4.0%; batches of 30 cells from $n = 3$ donors). However, the inhibitory effect of nocodazole was dependent on the time of drug application after nuclear injection: as the period before drug exposure lengthened, the ability of nocodazole to prevent cell surface expression decreased (Fig. 5*B*).

To assess the effects of these drugs on the rate of hRFC-EGFP expression at the plasma membrane, we measured the fluorescence intensity at the cell surface over time in the absence and presence of cytochalasin D or nocodazole. Prolonged incubation of oocytes with either drug resulted in characteristic changes in the morphology of the oocyte (6, 32). Cytochalasin D (10 μM) caused the pigment granules to aggregate into bundles, giving the oocyte a mottled appearance, whereas treatment with nocodazole (10 μM) resulted in the displacement of the germinal vesicle from within the animal hemisphere, causing a clearance of the pigment granules as it floated toward the surface (Fig. 5*C*). These morphological changes, although providing a useful control for drug efficacy, should be kept in mind when analyzing fluorescence intensities, because clearing of the pigment granules in itself results in increased detection of fluorescence from within the oocyte, especially during the initial period of drug application (data not shown). However, over longer time periods (Fig. 5*C*), the rate of increase of fluorescence at the cell surface stabilized and was estimated by measuring the gradient of the intensity profile. Figure 5*C* shows that the net rate of delivery of hRFC-EGFP to the membrane was identical in control (16.5 fluorescence units/h) and cytochalasin-D-treated (16.2 fluorescence units/h) cells but was approximately fourfold slower in nocodazole-treated cells (4.4 fluorescence units/h). Although disruption of microtubules slowed the rate of hRFC-EGFP trafficking, the asymmetric expression of hRFC-EGFP at the plasma membrane was unaffected in oocytes treated with nocodazole. The average animal-to-vegetal ratio was 13.7 ± 1.7 ($n = 10$ cells, 3 donors) after treatment with nocodazole for >24 h. Similarly, cytochalasin D was without affect on the polarity of hRFC-EGFP expression (animal-to-vegetal ratio of 17.5 ± 3.8; $n = 10$ cells, 3 donors).

DISCUSSION

The use of *Xenopus* oocytes as a model system for studying cell biology of membrane transporters has precedence (10, 14), having been selected as a model because of several advantages for studying intracellular trafficking and targeting of membrane proteins. First, the oocyte is an unusually large cell (~1-μl volume) with an extensive membrane surface area further enhanced by the plasma membrane microvilli that are especially enriched in the animal hemisphere (7, 46). The rate of vesicle trafficking to and from the plasma membrane is high (46), such that the system is ideal for observation of near-membrane trafficking events. Our visualization of hRFC-EGFP in vesicles moving through the ER toward the cell membrane (Fig. 2*D*) confirms the potential of the oocyte for trafficking studies. Second, *Xenopus* oocytes faithfully express exogenous proteins and target them to the correct cellular compartment. Finally, the *Xenopus* oocyte is a prototype polarized cell, displaying structural and functional asymmetry along an animal-vegetal axis specified during oogenesis (11, 42). Many endogenous membrane proteins are localized asymmetrically across the oocyte, with some preferentially expressed within the cell membrane of the animal hemisphere (16, 26), others within the cell membrane of the vegetal hemisphere (21, 30), and others distributed more uniformly (22). Similarly, exogenously expressed membrane proteins are targeted to the animal hemisphere (30, 32), the vegetal hemisphere (21), or throughout the entire oocyte surface (34, 38). Thus the cellular mechanisms that sort endogenous/exogenous proteins to different regions of the cell surface potentially can be exploited to investigate the molecular determinants that direct targeting of proteins to the cell membrane.

Our current interest in the cell biology and physiology of RFC relates to identifying the molecular signal(s)/motif(s) that guide the targeting of the protein to the plasma membrane and in assessing the role of the cytoskeleton in the intracellular trafficking of hRFC in different cell types. To begin addressing these issues, we used *Xenopus* oocytes directly injected into the nucleus with hRFC cDNA (39). In contrast to cRNA injection, this approach ensures that expressed protein will pass through the oocyte's endogenous machinery for transcription, translation, and trafficking, maintaining the effects of regulatory mechanisms active at the transcriptional and translational levels. Our results showed that *Xenopus* oocytes express functional hRFC-EGFP protein at the plasma membrane, with a greater peak fluorescence signal (~15-fold) in the ani-

mal compared with the vegetal pole. This asymmetric distribution of hRFC-EGFP is maintained for at least 7 days after injection (Fig. 1*C*), suggesting that polarity does not simply result from the closer spatial positioning of the oocyte nucleus to the animal pole (33) but is an actively maintained phenomenon. The asymmetric distribution of hRFC-EGFP at the cell surface did not result from an endogenous asymmetry of the oocyte cytoskeleton, because EYFP-actin and EGFP-tubulin were expressed with only slight differences between each hemisphere (Fig. 5).

To determine whether the membrane-targeting signal is located in the COOH-terminal cytoplasmic tail of the hRFC protein or in a sequence in the backbone region of the polypeptide, we engineered specific constructs of the hRFC polypeptide fused to EGFP that totally or partially lack the COOH-terminal cytoplasmic tail. We also generated a fusion protein of the COOH-terminal cytoplasmic tail of hRFC fused to EGFP (F2R1). Our results showed that partial or complete truncation of the COOH-terminal tail of hRFC has no effect on targeting of hRFC to the plasma membrane (Fig. 4*B*). The ratio of expression at the plasma membrane of animal and vegetal hemispheres, however, varied significantly from that observed with full-length hRFC-EGFP (Fig. 4*C*). With the completely truncated construct F1R3, weak expression was detectable in the vegetal pole (thereby decreasing the observed asymmetry), suggesting that the COOH-terminal tail of hRFC may play some role in asymmetric targeting of the protein to oocyte plasma membrane. However, with partial truncation of the COOH-terminal cytoplasmic tail (F1R2), enhancement of polarity over full-length protein was observed. This is possibly caused by a greater efficiency of trafficking or resistance to degradation. With the F2R1 construct, comprising the COOH-terminal cytoplasmic tail fused to EGFP, no fluorescence was found at the plasma membrane, suggesting that, if translated, the protein was not membrane targeted. These results suggest that for hRFC polypeptide, the membrane-targeting motif(s)/signal(s) is most likely located in the backbone sequence of the hRFC polypeptide, i.e., outside its COOH-terminal cytoplasmic tail. Further studies are required to determine the nature and specific location of the membrane-targeting motif(s)/signal(s) of the hRFC protein. Results similar to those described in this study were recently observed in our laboratory for membrane targeting of hRFC in mammalian cells (renal epithelial HEK-293 cells; unpublished observations).

Whereas previous work demonstrated a role for the cytoskeleton in intracellular trafficking of other membrane transporters (1, 4, 9, 13), little is known about the role played by the cytoskeleton in the intracellular trafficking of hRFC. In this study, we used nocodazole and cytochalasin D to investigate the respective roles of microtubules and the actin cytoskeleton in hRFC trafficking. Although both drug are effective in disrupting the oocyte cytoskeleton (6, 15), long-term (<50 h) incubation of oocytes with either drug does not impair cell viability, as assessed by measurements of membrane potential and resistance (32), membrane morphology (6), or synthesis of heterologous proteins (6, 32). Our results showed that incubation of oocytes with nocodazole markedly reduced the rate of expression of hRFC-EGFP at the animal pole (Fig. 5*C*) but not the polarity of hRFC-EGFP expression. When nocodazole was applied soon (3–6 h) after nuclear injection, many oocytes displayed no measurable fluorescence 30 h later (Fig. 5*B*). However, it was unclear whether this lack of fluorescence simply resulted from a complete inhibition of hRFC-EGFP transport or simply a slowed trafficking of hRFC-EGFP throughout the incubation period. In either case, these results demonstrate, for the first time, the importance of intact microtubules for intracellular hRFC trafficking. In contrast, disruption of actin filaments with cytochalasin D had little effect on hRFC-EGFP trafficking: the percentage of oocytes expressing hRFC-EGFP at the plasma membrane (Fig. 5*B*), the rate of hRFC trafficking (Fig. 5*C*), and the observed polarity were similar to those in control cells.

In summary, our results demonstrate that hRFC is targeted to the plasma membrane in *Xenopus* oocytes and is expressed asymmetrically across the cell. In addition, the molecular determinant(s) responsible for targeting the hRFC protein to the cell membrane in *Xenopus* oocytes resides within a sequence in the backbone of the polypeptide and not within the COOH-terminal cytoplasmic tail. Finally, an intact microtubule network appears to be essential for hRFC intracellular trafficking in the *Xenopus* oocyte. These results provide a basis for further investigations into the cell biology of trafficking and membrane targeting of hRFC in a variety of other cellular contexts.

This work was supported by the Department of Veterans Affairs and National Institutes of Health Grants DK-56061, DK-58057, and GM-48071. J. S. Marchant was supported by a Wellcome Trust Fellowship (no. 053102).

REFERENCES

1. **Achler C, Filmer D, Mertre C, and Drenckhahn D.** Role of microtubules in polarized delivery of apical membrane proteins to the brush border of the intestinal epithelium. *J Cell Biol* 109: 179–189, 1989.
2. **Alonso MA, Fan L, and Alarcon B.** Multiple sorting signals determine apical localization of a nonglycosylated integral membrane protein. *J Biol Chem* 272: 30748–30752, 1997.
3. **Blakley RL and Whitehead VA.** *Folates and Pterins. Nutritional, Pharmacological and Physiological Aspects.* New York: Wiley, 1986.
4. **Brown D.** Targeting of membrane transporters in renal epithelia: when cell biology meets physiology. *Am J Physiol Renal Physiol* 278: F192–F201, 2000.
5. **Caplan MJ.** Membrane polarity in epithelial cells: protein sorting and establishment of polarized membrane domains. *Am J Physiol Renal Physiol* 272: F425–F429, 1997.
6. **Colman A, Morser J, Lane C, Besley J, Wylie C, and Valle G.** Fate of secretory proteins trapped in oocytes of *Xenopus laevis* by disruption of the cytoskeleton or by imbalanced subunit synthesis. *J Cell Biol* 91: 770–780, 1981.
7. **Dascal N.** The use of *Xenopus* oocytes for the study of ion channels. *Crit Rev Biochem* 22: 317–387, 1987.
8. **Dixon KH, Lanpher BC, Chiu J, Kelley K, and Cowan KH.** A novel cDNA restores reduced folate carrier activity and meth-

otrexate sensitivity to transport deficient cells. *J Biol Chem* 269: 17–20, 1994.
9. **Dranoff JA, McClure M, Burgstahler AD, Denson LA, Crawford AR, Crawford JM, Karpen SJ, and Nathanson MH.** Short-term regulation of bile acid uptake by microfilament-dependent translocation of rat ntcp to the plasma membrane. *Hepatology* 30: 223–229, 1999.
10. **Due AD, Zhi-Chao Q, Thomas JM, Buchs A, Powers AC, and May JM.** Role of the C-terminal tail of the GLUT1 glucose transporter in its expression and function in *Xenopus la*evis oocytes. *Biochemistry* 34: 5462–5471, 1995.
11. **Dumont JN.** Oogenesis in *Xenopus laevis* (Daudin). I. Stages of oocyte development in laboratory maintained animals. *J Morphol* 136: 153–180, 1972.
12. **Ferguson PL and Flintoff WF.** Topological and functional analysis of the human reduced folate carrier by haemagglutinin epitope insertion. *J Biol Chem* 23: 16269–16278, 1999.
13. **Fletcher LM, Welsh GI, Oatey PB, and Tavare JM.** Role for the microtubule cytoskeleton in GLUT4 vesicle trafficking and in the regulation of insulin-stimulated glucose uptake. *Biochem J* 352: 267–276, 2000.
14. **Garcia JC, Strube M, Leingang K, Keller K, and Mueckler MM.** Amino acid substitutions at tryptophan 388 and tryptophan 412 of the HepG2 (Glut1) glucose transporter inhibit transport activity and targeting to the plasma membrane in *Xenopus* oocytes. *J Biol Chem* 267: 7770–7776, 1992.
15. **Gard DL, Cha BJ, and King E.** The organization and animal-vegetal asymmetry of cytokeratin filaments in stage VI *Xenopus* oocytes is dependent upon F-actin and microtubules. *Dev Biol* 184: 95–114, 1997.
16. **Gomez-Hernandez J-M, Stühmer W, and Parekh AB.** Calcium dependence and distribution of calcium-activated chloride channels in *Xenopus* oocytes. *J Physiol (Lond)* 502: 569–574, 1997.
17. **Gut A, Kappeler F, Hyka N, Balda MS, Hauri HP, and Matter K.** Carbohydrate-mediated Golgi to cell surface transport and apical targeting of membrane proteins. *EMBO J* 17: 1919–1929, 1998.
18. **Hernando N, Traebert M, Forster I, and Murer H.** Effect of two tyrosine mutations on the activity and regulation of the renal type II Na/P_i-cotransporter expressed in oocytes. *J Membr Biol* 168: 275–282, 1999.
19. **Karim-Jimenez Z, Hernando N, Biber J, and Murer H.** Requirement of a leucine residue for (apical) membrane expression of type IIb NaP_i cotransporters. *Proc Natl Acad Sci USA* 97: 2916–2921, 2000.
20. **Kumar CK, Nguyen TT, Gonzales FB, and Said HM.** Comparison of intestinal folate carrier clone expressed in IEC-6 cells and in *Xenopus* oocytes. *Am J Physiol Cell Physiol* 274: C289–C294, 1998.
21. **Levine E, Werner R, Neuhaus I, and Dahl G.** Asymmetry of gap junction formation along the animal-vegetal axis of *Xenopus* oocytes. *Dev Biol* 156: 490–499, 1993.
22. **Machaca K and Hartzell HC.** Asymmetrical distribution of Ca-activated Cl channels in *Xenopus* oocytes. *Biophys J* 74: 1286–1295, 1998.
23. **Marshall BA, Murata H, Hresko RC, and Mueckler MM.** Domains that confer intracellular sequestration of the Glut4 glucose transporter in *Xenopus* oocytes. *J Biol Chem* 35: 26193–26199, 1993.
24. **Mason JB and Rosenberg IH.** *Intestinal Absorption of Folate.* New York: Raven, 1994, p. 1979–1995.
25. **Matter K and Mellman I.** Mechanisms of cell polarity: sorting and transport in epithelial cells. *Curr Opin Cell Biol* 6: 545–554, 1994.
26. **Matus-Leibovitch N, Lupu-Meiri M, and Oron Y.** Two types of intrinsic muscarinic responses in *Xenopus* oocytes. *Pflügers Arch* 417: 194–199, 1990.
27. **Moscow JA, Gong M, He R, Sgagias MK, Dixon KH, Anzick SL, Mettzer PS, and Cowan KH.** Isolation of a gene encoding a human reduced folate carrier (RFC1) and analysis of its expression in transport-deficient, methotrexate-resistance human breast cancer cells. *Cancer Res* 55: 3790–3794, 1995.
28. **Muth TR, Ahn J, and Caplan MJ.** Identification of sorting determinants in the C-terminal cytoplasmic tails of the γ-aminobutyric acid transporters GAT-2 and GAT-3. *J Biol Chem* 40: 25616–25627, 1998.
29. **Nguyen TT, Dyer DL, Dunning DD, Rubin SA, Grant KE, and Said HM.** Human intestinal folate transport: cloning, expression, and distribution of complementary RNA. *Gastroenterology* 112: 783–791, 1997.
30. **Oron Y, Gillo B, and Gershengorn MC.** Differences in receptor-evoked membrane electrical responses in native and mRNA-injected *Xenopus* oocytes. *Proc Natl Acad Sci USA* 85: 3820–3824, 1988.
31. **Parker I, Callamaras N, and Wier WG.** A high-resolution, confocal laser-scanning microscope and flash photolysis system for physiological studies. *Cell Calcium* 21: 441–452, 1997.
32. **Peter AB, Schittny JC, Niggli V, Reuter H, and Sigel E.** The polarized distribution of the poly(A+)-mRNA-induced functional ion channels in the *Xenopus* oocyte plasma membrane is prevented by anticytoskeletal drugs. *J Cell Biol* 114: 455–464, 1991.
33. **Pfeiffer DC and Gard DL.** Microtubules in *Xenopus* oocytes are orientated with their minus-ends towards the cortex. *Cell Motil Cytoskeleton* 44: 34–43, 1999.
34. **Roberts SJ, Leaf DS, Moore H-P, and Gerhart JC.** The establishment of polarized membrane traffic in *Xenopus laevis* embryos. *J Cell Biol* 118: 1359–1369, 1992.
35. **Said HM and Kumar C.** Intestinal absorption of vitamins. *Curr Concept Gastroenterol* 15: 172–176, 1999.
36. **Said HM, Rose R, and Seetharam B.** *Intestinal Absorption of Water-Soluble Vitamins: Cellular and Molecular Aspects.* San Diego: Academic, 2000, p. 35–75.
37. **Sirotnak FM and Tolner B.** Carrier-mediated transport of folates in mammalian cells. *Annu Rev Nutr* 19: 91–122, 1999.
38. **Sweet DH, Miller DS, and Pritchard JB.** Basolateral localization of organic cation transporter 2 in intact renal proximal tubules. *Am J Physiol Renal Physiol* 279: F826–F834, 2000.
39. **Swick AG, Janicot M, Cheneval-Kastelic T, McLenithan JC, and Lane MD.** Promoter-cDNA directed heterologous expression in *Xenopus laevis* oocytes. *Proc Natl Acad Sci USA* 89: 1812–1816, 1992.
40. **Titus SA and Moran RG.** Retrovirally mediated complementation of the glyB phenotype. *J Biol Chem* 275: 36811–36817, 2000.
41. **Tsien RY.** The green fluorescent protein. *Annu Rev Biochem* 67: 509–544, 1998.
42. **Ubbels GA.** Establishment of polarities in the oocyte of *Xenopus laevis*: the provisional axial symmetry of the full-grown oocyte of *Xenopus laevis*. *Cell Mol Life Sci* 53: 382–409, 1997.
43. **Williams FMR and Flintoff WF.** Isolation of a human cDNA that complements a mutant hamster cell defective in methotrexate uptake. *J Biol Chem* 270: 2987–2992, 1995.
44. **Williams FMR, Murray RC, Underhill TM, and Flintoff WF.** Isolation of a hamster cDNA clone coding for a function involved in methotrexate uptake. *J Biol Chem* 269: 5810–5816, 1994.
45. **Wong SC, Proefke SA, Bhusan A, and Matherly LH.** Isolation of human cDNAs that restore methotrexate sensitivity and reduced folate carrier activity in methotrexate transport-defective Chinese hamster ovary cells. *J Biol Chem* 270: 17468–17475, 1995.
46. **Zampighi GA, Loo DDF, Kreman M, Eskandari S, and Wright EM.** Functional and morphological correlates of Connexin50 expressed in *Xenopus laevis* oocytes. *J Gen Physiol* 113: 507–523, 1999.